Progress of Theoretical Physics, Vol. 82, No. 3, September 1989

# Gravitational Radiation from Coalescing Binary Neutron Stars. I

Ken-ichi OOHARA and Takashi NAKAMURA

*National Laboratory for High Energy Physics, Tsukuba 305*

(Received May 29, 1989)

We have performed numerical simulations of coalescence of a binary system consisting of two neutron stars using a Newtonian hydrodynamics code, which is constructed adopting LeBlanc's method for a transport term with tensor artificial viscosity terms to express shock waves. We use a Cartesian coordinate system $(x, y, z)$ and take typically a $141\times141\times141$ grid. The code passed various test-bed problems. Calculation is started when two neutron stars just contact with each other. We use a polytropic equation of state with $\gamma=2$ to express high density matter and the amount of gravitational waves is estimated using a quadrupole formula. For the coalescence of two neutron stars of each mass 1.4 $M_\odot$, the total energy radiated during the first 1.9 msec can be 2.7% of the rest mass, which is much larger than any estimates of the burst sources of the gravitational waves. The luminosity in the final stage of our calculation is still high. This fact indicates that simulation including the back reaction is urgent to know the final destiny. Wave patterns as well as energy spectra of gravitational waves are also shown.

## § 1. Introduction

Coalescence of a binary system consisting of two neutron stars or black holes has been considered to be one of the strongest sources of the gravitational radiation. Several analyses have been performed to estimate the total energy of the gravitational waves emitted in process of the coalescence. Gilden and Shapiro[1] calculated the head-on collision of two neutron stars using a Newtonian hydrodynamics code and obtained the typical efficiency ($\Delta E/M$) being 0.1% for colliding 1.4 $M_\odot$ neutron stars. This efficiency is comparable to the result for the head-on collision of two black holes ($\leq$0.1%) by Smarr[2] and for the formation of rotating black holes ($\leq$0.1%) by Stark and Piran[3] using fully general relativistic codes. These results suggest that the total energy radiated from an axially symmetric system is at most 0.1% of the rest mass. However it was only axially symmetric systems that were considered in these calculations.

Nakamura, Oohara and Kojima[4] studied extensively the efficiency of the emission of the gravitational waves from a test particle falling into a Schwarzschild or a Kerr black hole. They found the efficiency for an axially symmetric system is generally much smaller than that for a non-axially symmetric system because of the phase cancellation effects. Extrapolating their results of perturbation calculations to non-axisymmetric coalescence of two identical black holes, the efficiency increases at least to 0.3% and can reach 9% depending on spin and orbital angular momenta of black holes. As for the coalescence of a binary neutron star, Clark and Eardley[5] studied the evolution of a binary system consisting of two neutron stars of mass 1.3 $M_\odot$ and 0.8 $M_\odot$ and estimated the gravitational waves emitted in the stable mass stripping phase. They showed that the total energy of the gravitational waves is $6\times10^{52}$ ergs, which is 1.5% of the rest mass.

Up to the present, 10 binary pulsars are observed. Two of them have a large

eccentricity and a large mass companion ($\sim 1.4\ M_\odot$), while the rests have a small eccentricity and a small mass companion ($\leq 0.4\ M_\odot$). In particular, PSR1913+16 has been observed precisely and it is believed to consist of two neutron stars of mass 1.445 $M_\odot$ and 1.384 $M_\odot$.[6] Two neutron stars in PSR1913+16 will coalesce in $\sim 10^8$ y because of the emission of gravitational waves. The binary millisecond pulsar PSR 0021−72A,[7] which has been recently discovered, will coalesce in a much shorter time $\sim 10^6$ y. Under the assumption of a steady state, the frequency in coalescence of binary neutron stars is estimated at $\sim 10$ events/year within the distance of 100 Mpc. Therefore they can be important sources of gravitational waves.

Another kind of coalescence of neutron stars is theoretically expected to exist.[8] If the core of the progenitor of Type II supernova has a large angular momentum, the centrifugal force will be important in some stages of the collapse into a final neutron star. The core radius where the centrifugal force is comparable to the gravitational force is proportional to the square of the angular momentum. When the size of the core decreases to this radius the core contracts principally along the rotational axis and then a thin disk will be formed. Such a thin disk is known to be gravitationally unstable irrespective of the equation of state[9] and fragments into several pieces in a free fall time scale. Each fragment looks like a neutron star and is called a proto neutron star. Proto neutron stars will coalesce again to form a single neutron star owing to the emission of gravitational waves. If the number of fragments is two, the system is essentially the same as a binary like PSR1913+16 in the final coalescence stage. A time profile of neutrino events,[8] a sub-millisecond pulsar[10] and the existence of a Jupiter-like secondary[11] suggest that this kind of process really occurred in SN1987A. If the scenario like this applies to all of Type II supernovae, the frequency in the events of burst emission of gravitational waves within the distance of 10 Mpc increases to $\sim 30$ events/year. Then it is urgent to estimate the amount, the wave pattern and the spectrum of the gravitational waves emitted in coalescence of a binary system of two neutron stars.

In this paper we present results of three-dimensional numerical simulations for coalescence of binary systems consisting of two neutron stars using a Newtonian hydrodynamics code. The emitted gravitational waves are estimated using the quadrupole formula. In § 2 we describe formulation and numerical methods. In § 3 results of simulations are presented and § 4 is devoted to discussion and astrophysical implications of the results.

## § 2. Formulation and numerical methods

The basic equations we use are the three-dimensional hydrodynamics equations given by

$$\frac{\partial \rho}{\partial t}+\frac{\partial \rho v^j}{\partial x^j}=0\,, \tag{2·1}$$

$$\frac{\partial \rho v^i}{\partial t}+\frac{\partial \rho v^i v^j}{\partial x^j}=-\frac{\partial P}{\partial x^i}-\rho\frac{\partial \psi}{\partial x^i}\,, \tag{2·2}$$

$$\frac{\partial \rho\varepsilon}{\partial t}+\frac{\partial \rho\varepsilon v^j}{\partial x^j}=-P\frac{\partial v^j}{\partial x^j}, \tag{2·3}$$

$$P=(\gamma-1)\rho\varepsilon \tag{2·4}$$

and

$$\Delta\psi=4\pi G\rho, \tag{2·5}$$

where all the variables have usual meanings. To express a hard equation of state, we use a polytropic equation of state with $\gamma=2$. We put initially two spherical neutron stars of mass $M_0$ and radius $r_0$ at $y=\pm r_0$ on the $y$-axis, which means that we start calculation when two neutron stars just contact with each other. As for the initial velocity we assume that

$$v_x=-y\Omega, \quad v_y=x\Omega \quad \text{and} \quad \Omega=0.5\sqrt{\frac{GM_0}{r_0{}^3}}q, \tag{2·6}$$

where $q$ is a parameter specifying the total angular momentum of the system. Here the system is assumed to be rigidly rotating with respect to the origin $x=y=z=0$. For $\gamma=2$, the pressure is expressed as

$$P=K\rho^2, \tag{2·7}$$

where $K$ is constant at $t=0$. Then $K$ is determined from the equilibrium solution as

$$K=\frac{2r_0{}^2G}{\pi}. \tag{2·8}$$

If we take the units of

$$L=\frac{C_s}{\sqrt{G\rho_c}}, \quad M=M_0 \quad \text{and} \quad T=\frac{1}{\sqrt{G\rho_c}}, \tag{2·9}$$

where $\rho_c$ and $C_s$ are respectively the density and the sound velocity at the center of each star, then the system is characterized by only one parameter $q$. This means that we can derive various solutions for different $M_0$ from one solution with a given $q$ by means of the scaling law. For comparison with results of fully general relativistic calculations in future, however, we adopt the following units,

$$M=M_\odot, \quad L=\frac{GM_\odot}{c^2}=1.5\ \text{km}, \quad T=\frac{GM_\odot}{c^3}=5\times10^{-6}\ \text{sec}. \tag{2·10}$$

To express the neutron star appropriately, we fix $r_0=6$ in our units, which means the radius of the neutron star is 9 km irrespective of mass $M_0$.

We will estimate the amount of gravitational radiation emitted using the quadrupole formula, which requires the third time derivatives of the quadrupole moment. However it is not so easy to maintain a good accuracy in performing three times a direct numerical differentiation of the quadrupole moment obtained from numerical results. Instead of the direct method, we adopt the following two methods.[12] First we reduce the first time derivative of the quadrupole moment to

$$\dot{D}_{ij}=\int\rho(x^iv^j+x^jv^i)dV\,, \tag{2·11}$$

using the continuity equation. Performing twice a numerical differentiation of this quantity, we obtain the third time derivative. We call the energy flux obtained using this method FLUX1. Furthermore with the aid of the equation of motion, the second time derivative of the quadrupole moment can be written as

$$\ddot{D}_{ij}=\int\left\{2\rho v^iv^j+2P\delta_{ij}-\rho\left(\frac{\partial\psi}{\partial x^i}x^j+\frac{\partial\psi}{\partial x^j}x^i\right)\right\}dV\,. \tag{2·12}$$

Although the integrand in Eq. (2·12) contains $\psi$, we do not need to integrate up to infinity because $\rho$ is multiplied to the potential terms. A numerical differentiation of Eq. (2·12) gives the third time derivatives. We call the energy flux obtained using this method FLUX2. Note that we use the traceless part of the third time derivatives of $D_{ij}$ to calculate the luminosity. In general cases FLUX2 is not noisy while FLUX1 has noisy fluctuations around a smooth curve of FLUX2 as shown in Nakamura and Oohara.[13] As a test of these methods, we calculated the flux emitted in collapse of homogeneous ellipsoid and compared the results with the semi-analytic ones.[14),15] (See Appendix B.) This fluctuation is caused by the truncation error of the numerical method and hence we use only FLUX2 in this paper.

We adopt a Cartesian coordinate system $(x, y, z)$ for three-dimensional hydrodynamics code. For the hydrodynamics code with the finite difference method, one of the major problems is how to treat the advection terms. LeBlanc has recently proposed a simple second order method for advection.[16] (Details of this method will be described in Appendix A.) Both a box type and a Gaussian type density distribution are successfully transported with his method and hence we adopt LeBlanc's method for the advection terms. To express shock waves we use the tensor artificial viscosity terms given by

$$Q_{ij}=\rho l^2\frac{\partial v^k}{\partial x^k}\left(\frac{\partial v^i}{\partial x^j}+\frac{\partial v^j}{\partial x^i}-\frac{2}{3}\delta_{ij}\frac{\partial v^n}{\partial x^n}\right)\quad\text{if}\quad\frac{\partial v^k}{\partial x^k}<0\,. \tag{2·13}$$

We use $\tilde{P}_{ij}\equiv P\delta_{ij}+Q_{ij}$ for the pressure tensor instead of the gas pressure $P$. This artificial viscosity terms with LeBlanc's transport term expresses a one-dimensional shock tube problem as well as a point explosion quite accurately. We solve the Poisson equation using an ICCG method described by Oohara and Nakamura.[17] We have performed an extensive series of test-bed calculations, which will be described briefly in Appendix B.

## § 3. Results

We take a $141\times141\times141$ grid. We performed six simulations with $q=0.0$, 0.25, 0.35, 0.5, 0.70 and 0.8. A typical CPU time per one time step is about 2 seconds on Hitachi S 820/80. We performed the numerical calculation for each model until $t=550$ in our units and the total CPU time needed for one model is typically 40000 seconds. We set $M_0=0.7\,M_\odot$ for all models and the total mass is $1.4\,M_\odot$, which means that each model corresponds to a binary formed in the rapidly rotating core collapse

in Type II supernova. However as was pointed out in the previous section, a simple scaling of the various physical quantities gives the results for $M_0=1.4\,M_\odot$ from the present numerical simulations.

We show in Figs 1(a)~(j) the contours of density and the velocity vectors on $x$-$y$, $y$-$z$ and $z$-$x$ planes for $q=0.5$. Solid lines are drawn at intervals of a tenth of the maximum density. Inner and outer dashed lines indicate respectively 19/20 and 1/20 of the maximum density. Figure 1(a) is the almost initial stage when two neutron stars just contact with each other. At $t=6$ (Fig. 1(b)) two stars rotate in about 30 degrees and the coalescence begins in the central region on account of the tidal gravitational force. The views of $y$-$z$ and $z$-$x$ planes show that an expanding motion along $z$-axis appears in the coalescing region. At $t=36$ (Fig. 1(c)) the coalescence seems to be completed in the central region temporarily. The rate of contraction in the central region is greater than in the outer region and then the angular velocity of the central part is made larger by the conservation of angular momentum. Consequently the shape of the density contour in the inner part rotates in advance of the outer part. In the views of $y$-$z$ and $z$-$x$ planes, we see the expansion along the $z$-axis and the contraction along $x$- and $y$-axes. At $t=52$ (Fig. 1(d)), however, the central part begins to expand again. The contraction in the previous stage makes the centrifugal force increase and the centrifugal force overcomes the gravity in this stage. This expansion causes the decrease in the angular velocity. Then the contours of density have almost the same phase. At the same time the jet motion along the $z$-axis becomes small. The expansion continues at the time of Fig. 1(e). Finally each neutron star appears again at $t=72$ (Fig. 1(f)). The motion in $y$-$z$ and $z$-$x$ planes seems to be stopped temporarily. In the next stage (Fig. 1(g)) the coalescence starts again because of the decrease in the centrifugal force and the contraction along $z$-axis begins again. At $t=96$ (Fig. 1(h)) the coalescence stops temporarily but at $t=112$ (Fig. 1(i)) the central part expands again. After this kind of oscillation continues several times, the system settles down to be a rotating bar shown in Fig. 1(j) at $t\sim300$. The final stable configuration is not due to the viscosity but to the redistribution of the angular momentum of each fluid element since the specific angular momentum is not conserved in a non-axially symmetric system. Although the shape in the cross section of the $x$-$y$ plane is a bar, the oscillation along the $z$-axis still continues. The formation of bar appears in all the models except for $q=0$. In general the larger is the angular momentum, the larger is the size of the bar.

We show the second time derivatives of quadrupole moment in Fig. 2 for $q=0.5$. Solid, dashed and dotted lines in the upper figure show respectively $\ddot{D}_{xx}$, $\ddot{D}_{yy}$ and $\ddot{D}_{xy}$, while $\ddot{D}_{zz}$ is shown in the lower figure. Both $\ddot{D}_{xz}$ and $\ddot{D}_{yz}$ vanish on account of the symmetry. Before $t=300$, all of $\ddot{D}_{ij}$ are irregular according to the transient phenomena before the formation of the final rotating bar. After $t=300$, however, $\ddot{D}_{xx}$, $\ddot{D}_{yy}$ and $\ddot{D}_{xy}$ oscillate with almost the same frequency but different phases. This is caused by the fact that the motion in the $x$-$y$ plane is governed by a rotating bar. The oscillation of $\ddot{D}_{zz}$, on the other hand, reflects the expansion and contraction of the matter along the $z$-axis shown in Fig. 1. The angular frequency of this oscillation ($\sim0.08$) is different from the rotation frequency in the $x$-$y$ plane ($\sim0.1$). The wave form of the gravitational radiation is obtained from the second derivative of the

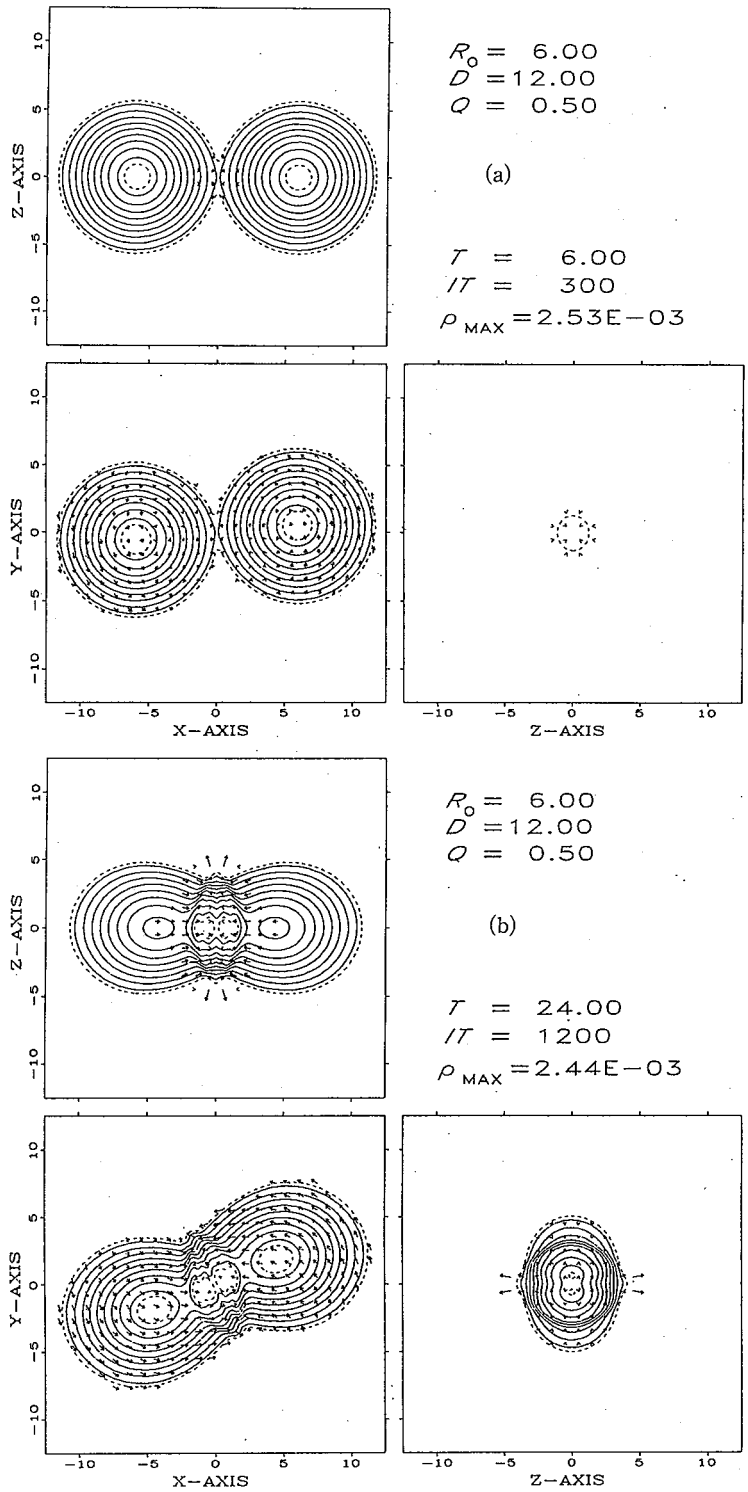


Fig. 1. Density contours on the $x$-$y$, $y$-$z$ and $z$-$x$ planes for $q$=0.5. The time $t$ and time step number $IT$ are indicated. The solid line is drawn by step of a tenth of the maximum density and the inner and the outer dashed lines indicate 19/20 and 1/20 of maximum density, respectively. The arrows indicate the velocity vectors of the matter.

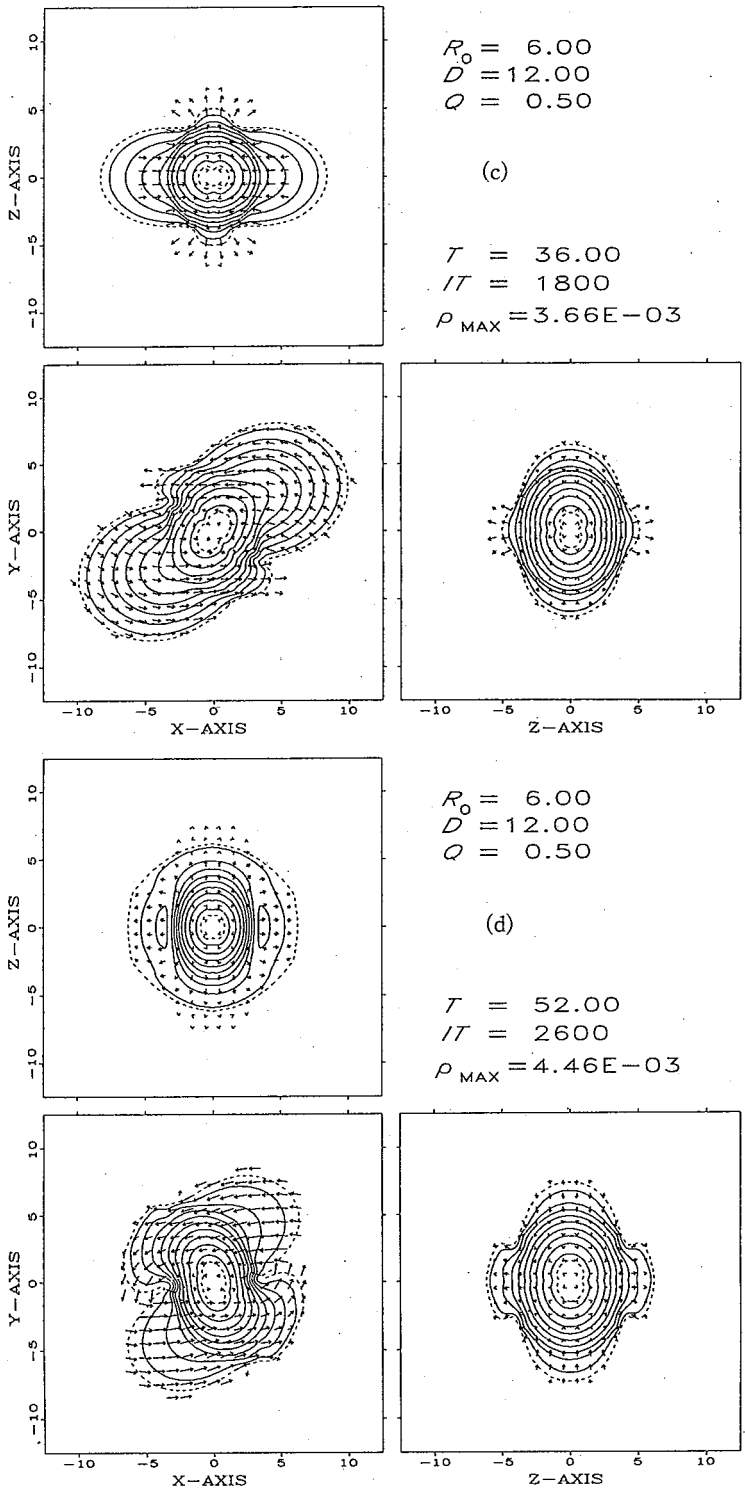


Fig. 1. (continued)

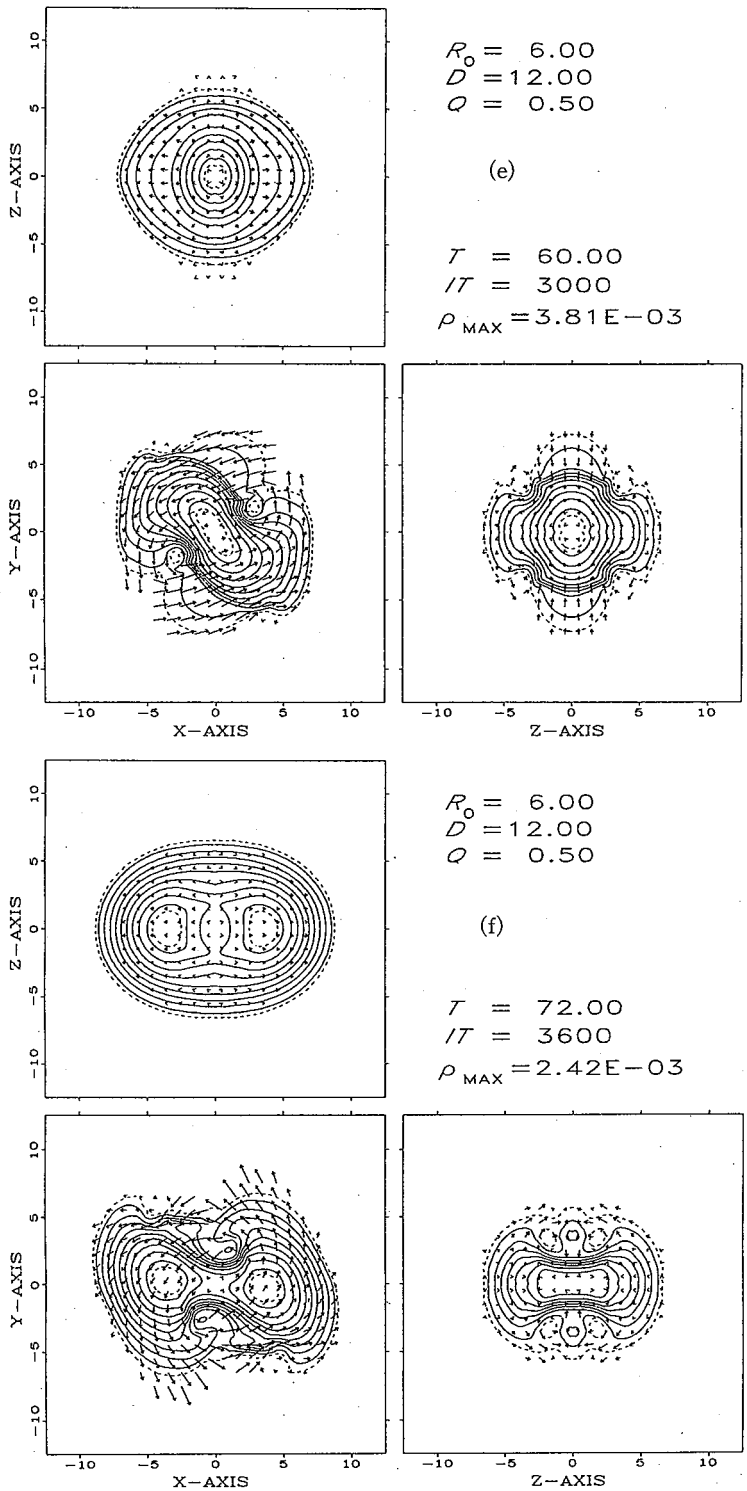


Fig. 1. (continued)

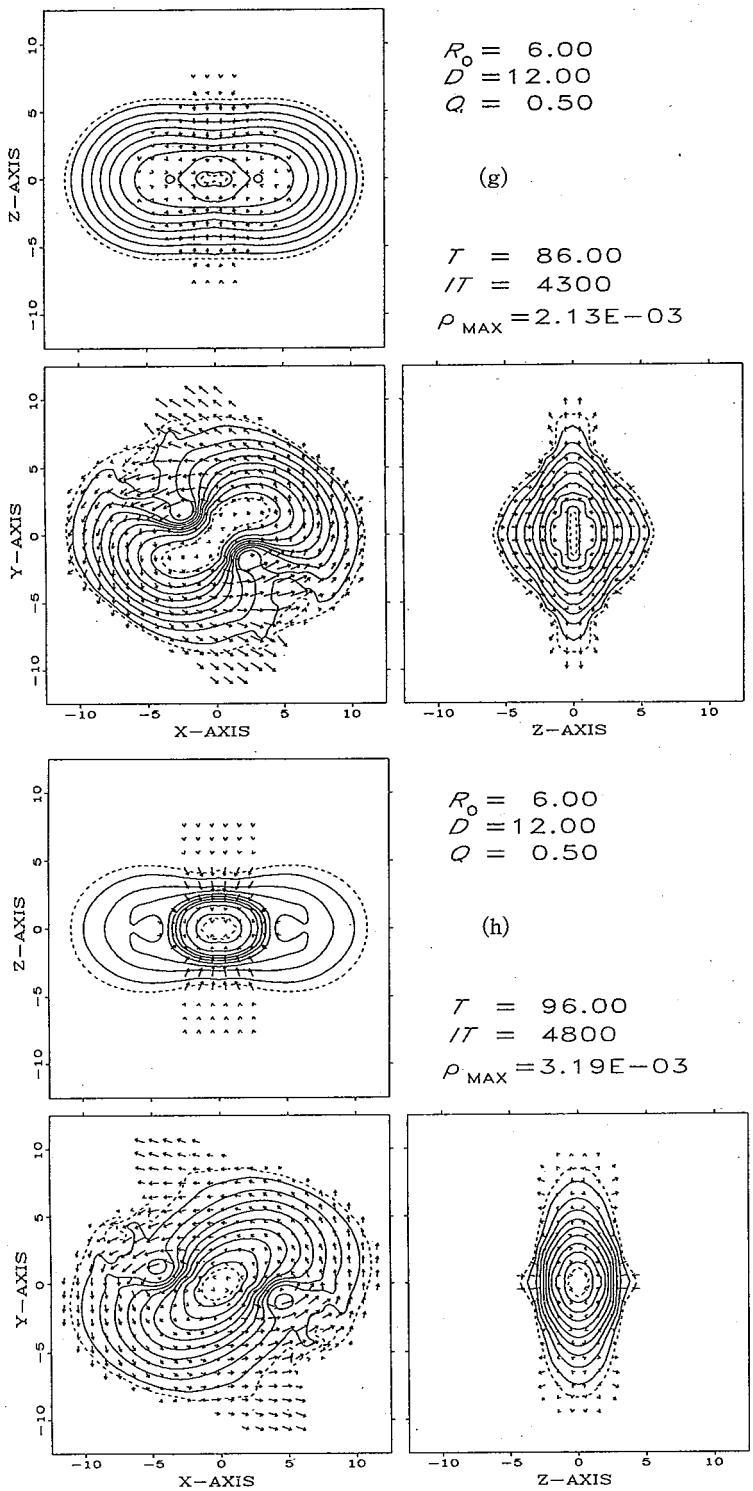


Fig. 1. (continued)

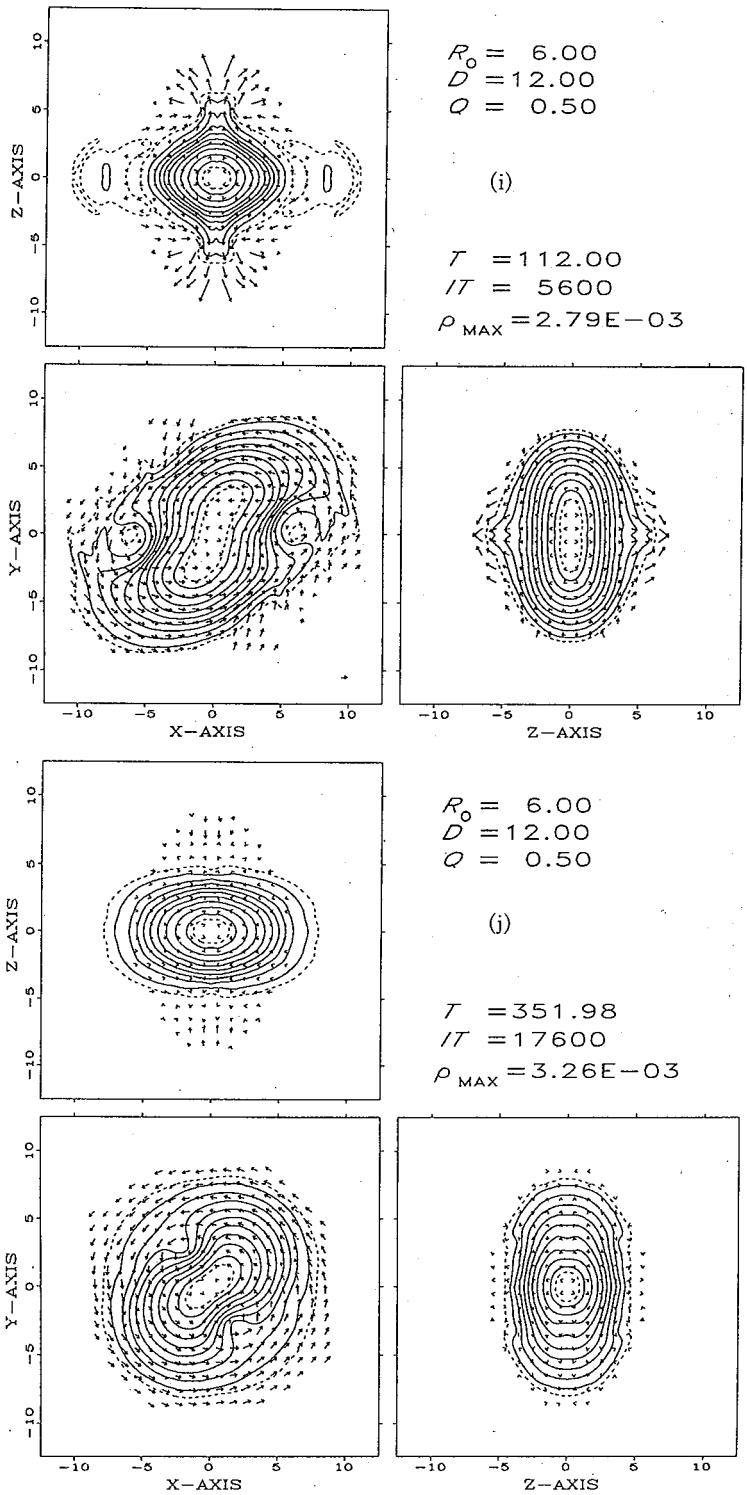


Fig. 1. (continued)

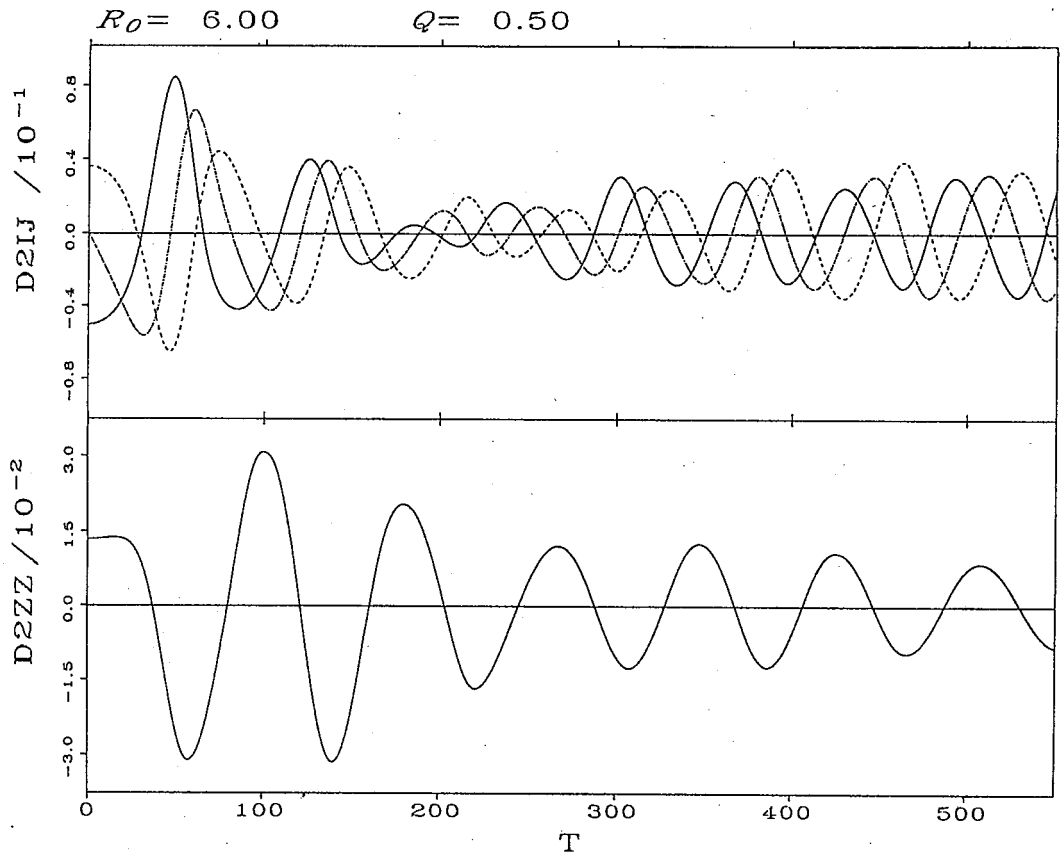


Fig. 2. Time profile of the second derivative of the quadrupole moment $\ddot{D}_{ij}$ for $q=0.5$. The solid, dashed and dotted lines in the upper figure show $\ddot{D}_{xx}$, $\ddot{D}_{yy}$ and $\ddot{D}_{xy}$, respectively. The lower figure is of $\ddot{D}_{zz}$.

quadrupole moment. We show the wave form observed on the $z$-axis in Fig. 3, where

$$h_+=\frac{1}{r}(\ddot{D}_{xx}-\ddot{D}_{yy}),$$

$$h_\times=\frac{2}{r}\ddot{D}_{xy}. \qquad (3\cdot1)$$

The wave pattern consists of two parts; 1) the transient oscillation and rotation at $t \leq 300$ and 2) the regular pattern at $t \geq 300$.

In Fig. 4 we show the energy spectra for $q=0.25$, 0.35, 0.5 and 0.8. The spectrum for $q=0.5$ has two peaks at $\omega=0.08$ and $\omega=0.1$, which correspond to the frequency of the rotation of the bar and the oscillation along the $z$-axis, respectively. Two peaks also appear for $q=0.8$. However for $q=0{:}35$ or 0.25 two frequencies of the oscillation are almost the same and then only one peak appears in the energy spectrum. In Fig. 5 we show the energy flux and the central density $\rho_c$ as functions of time. The central density $\rho_c$ begins to increase when the coalescence starts but the increase stops at $t \sim 50$ (Fig. 1(d) and (e)). At $t=90$ (Fig. 1(g)), $\rho_c$ starts to increase again. After several

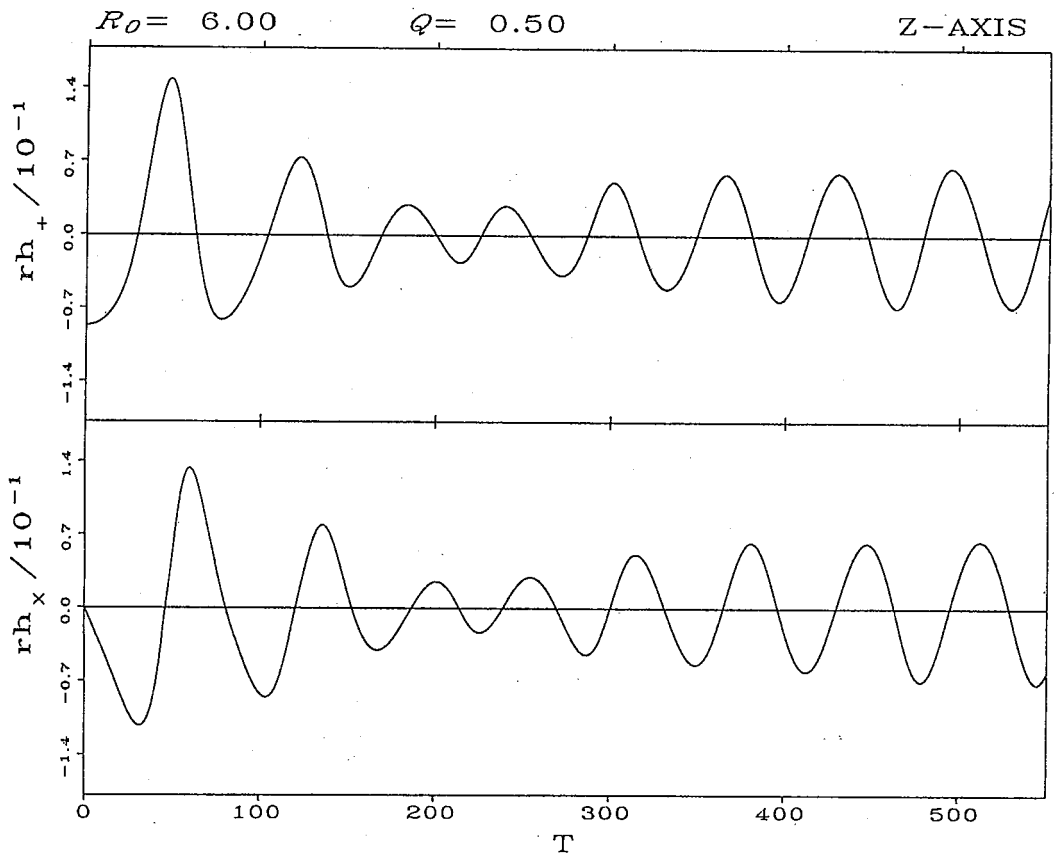


Fig. 3. Wave forms of $h_+$ and $h_\times$ observed on the $z$-axis for $q=0.5$.

cycles of such an oscillation, a variation of $\rho_c$ becomes rather regular. This is also caused by the regular oscillation along the $z$-axis. The variation of flux is not the same as that of the density. Nevertheless the flux gets to its local maximum when the increase of the central density stops except for some cases. This means that a lot of gravitational waves will be emitted when the motion is turned from collapse to expansion by the centrifugal force or the pressure.

The dependence of the total energy radiated up to $t=550$ on the angular momentum parameter $q$ is shown in Fig. 6. The largest energy ($3.19\times10^{-3}$ in our units) is emitted for $q=0.35$. This value means that the energy emitted up to 2.75 msec is $5.7\times10^{51}$ ergs or 0.23% of the rest mass for the coalescence of two neutron stars of each mass $0.7\,M_\odot$.

## § 4. Discussion

In every case except for $q=0$, the luminosity of the gravitational waves gets regular after a certain time since the bar like star is formed and is rotating almost rigidly. Thus we judged that we need not continue our calculation further. In

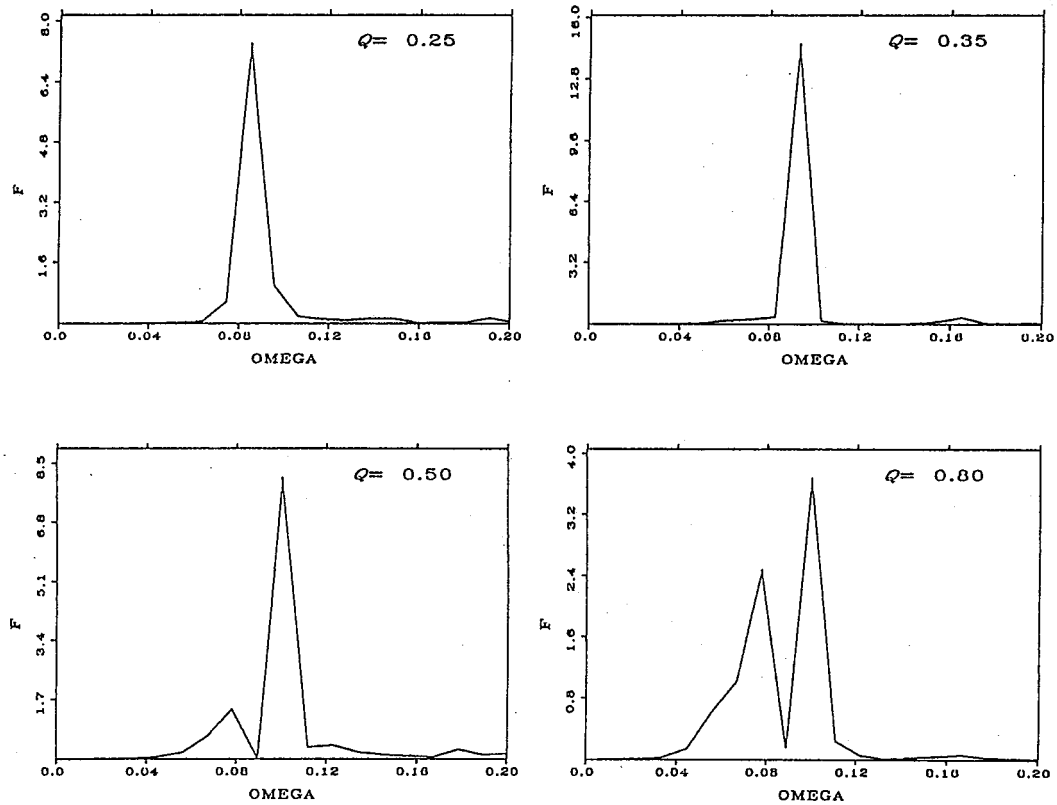


Fig. 4. Power spectra of $\dot{h}$ observed on the $z$-axis for $q=0.25$, 0.35, 0.5 and 0.8.

reality the system should not settle down to a steady state on account of the loss of the energy and the angular momentum. If the angular momentum is lost, the system gets smaller because of the decrease in the centrifugal force. However it is not obvious whether the angular velocity of the bar increases or decreases, since the moment of inertia also decreases at the same time. If the effect of the decrease in the moment of inertia overcomes the loss of the angular momentum, the angular velocity will increase. Since the luminosity of the gravitational waves is proportional to the square of the moment of inertia and the sixth power of the angular velocity, it is possible for the luminosity to increase with the loss of the angular momentum. In a decay of a binary system consisting of two point particles, the moment of inertia and the angular velocity are proportional to $a^2$ and $a^{-3/2}$, respectively, where $a$ is the separation of the particles, and hence the luminosity will increase as $a^{-5}$ with the loss of the angular momentum. This fact points out that calculations including the effect of back reaction are needed to know the final destiny of the system.

In the framework of the quadrupole formula, the radiation reaction potential is given by the fifth time derivatives of the quadrupole moment.[17] A simple method of taking into account the radiation reaction is to calculate the fifth derivatives and including them in the equations of motion though there are some theoretical questions, such as the gauge conditions and the existence of a lot of time constants, about applying such a simple reaction potential to our system. If we solve two more

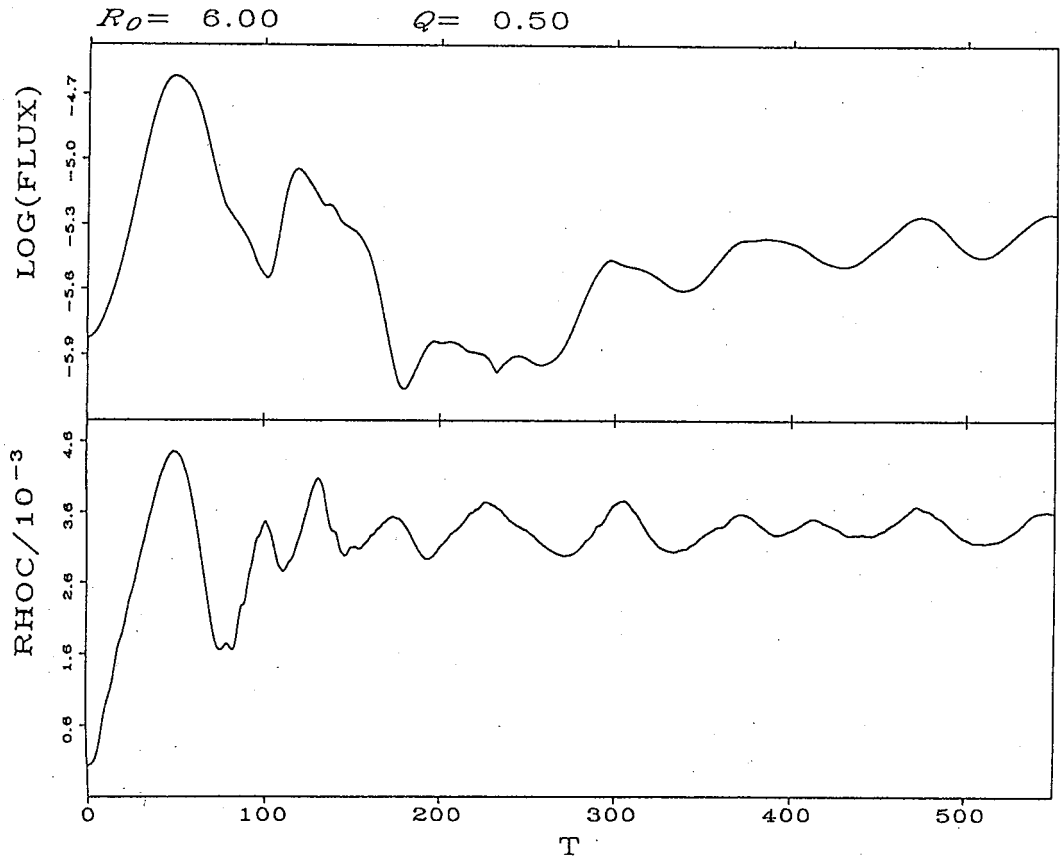


Fig. 5. Luminosity (FLUX2) and central density $\rho_c$ as functions of time $t$ for $q=0.5$. The upper figure shows log (FLUX2) and the lower figure does $\rho_c$.

Poisson equations, it is possible to estimate accurately the fifth time derivatives of the quadrupole moment. First, let us consider the time derivative of Eq. (2·12). With the aid of the equation of motion, the continuity and the energy equations, all the time derivatives except for $\dot{\psi}$ are converted to the spatial derivatives. We will thus obtain a smooth third derivatives of $D_{ij}$, if $\dot{\psi}$ is calculated accurately. The quantity $\dot{\psi}$ obeys

$$\begin{aligned}\Delta\dot{\psi} &= 4\pi G\dot{\rho} \\ &= -4\pi G\,\mathrm{div}(\rho \boldsymbol{v})\,. \end{aligned} \tag{4·1}$$

Here we used the continuity equation to eliminate the time derivative $\dot{\rho}$ from the source term. Solving this Poisson equation, we obtain the accurate values of $\dddot{D}_{ij}$.

To calculate the fourth derivatives we repeat the above procedure. Time derivatives can be eliminated from the source term in the Poisson equation for $\ddot{\psi}$ also with the aid of the equation of motion. We tried to estimate the fifth time derivative of the quadrupole moment using this method. A comparison was made for the collapse of the homogeneous ellipsoid between the results obtained using this method and those obtained from solving ordinary differential equations, which will be shown in Appendix B, and we confirmed the results are satisfactory. Then we performed

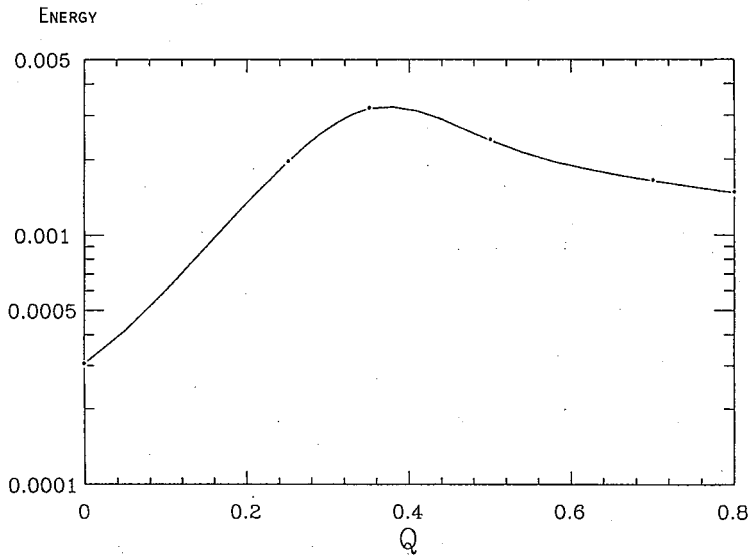


Fig. 6. Total energy of the gravitational waves emitted as a function of the angular momentum parameter $q$.

several preliminary computations with back reaction potentials. No numerical instabilities appeared. Thus simulations using finer grids are urgent. However needless to say we need much more CPU time since we solve three Poisson equations for each time step.

The most accurate method of performing a simulation of the coalescence of a binary system consisting of neutron stars is to construct a fully general relativistic code, in which the back reaction is included. We are now extending the hydrodynamics code presented in this paper to the general relativistic code making use of the three-dimensional metric code constructed for the pure gravitational waves.[13]

Finally we apply our results for $q=0.35$ to the coalescence of the binary neutron star system with each mass 1.4 $M_\odot$ and each radius 9 km. From the scaling law discussed in § 2, the total energy radiated scales as $M^{4.5}$. Thus $1.3\times10^{53}$ ergs is radiated as the gravitational waves in the first 1.93 msec. This value amounts to 2.7% of the rest mass of the system. As a demonstration we show in Fig. 7 the wave pattern from a hypothetical source of a coalescing binary of each mass 1.4 $M_\odot$ in the Virgo cluster (10 Mpc). The non-dimensional amplitude of the gravitational wave $h$ becomes $1.2\times10^{-21}$, which may be detected with next generation gravitational wave detectors in 1990's.

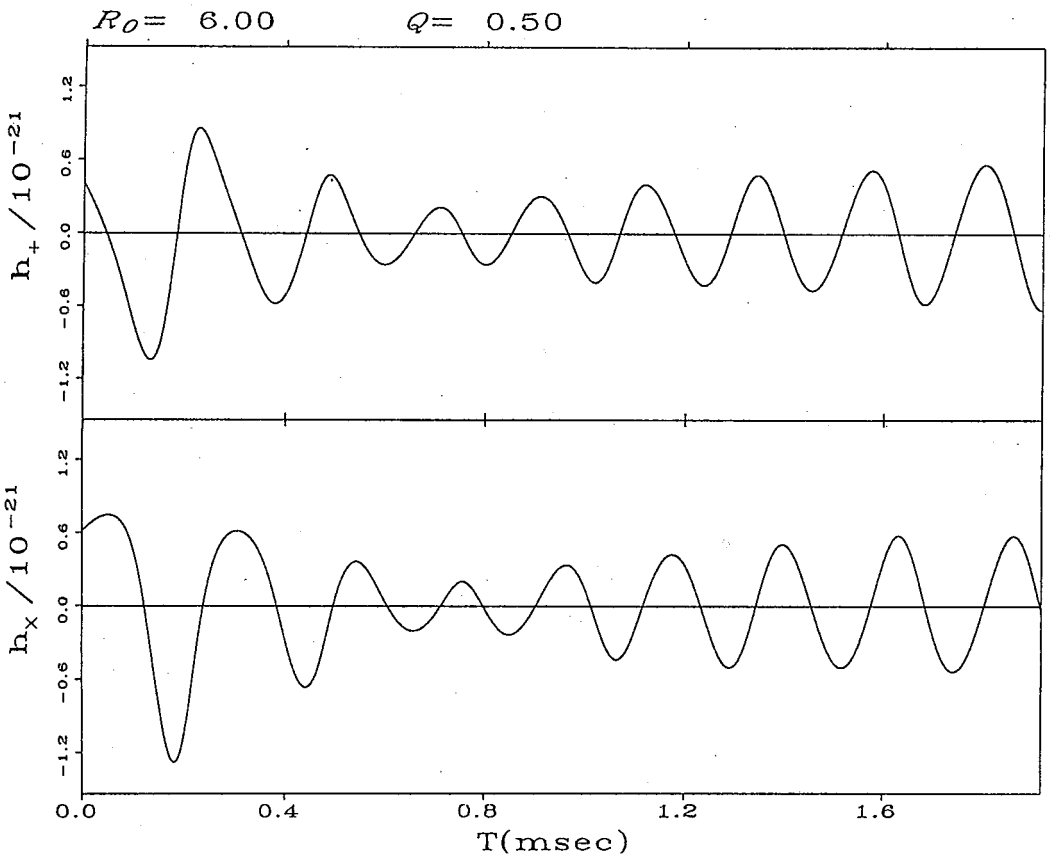


Fig. 7. Wave forms $h_+$ and $h_\times$ emitted in coalescence of two neutron stars of mass 1.4 $M_\odot$ with $q=0.5$ observed at the point of distance $r=10$ Mpc, latitude $\theta=30°$ and longitude $\phi=60°$.

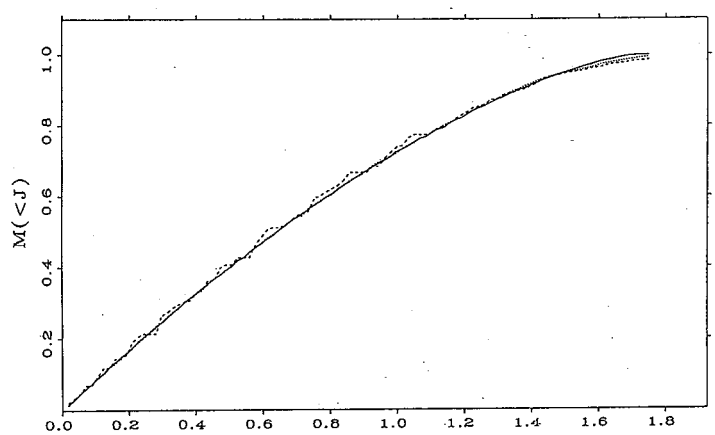


Fig. 8. The mass $M(J)$ with specific angular momentum less than or equal to $J$ as a function of $J$. The solid line indicates $M(J)$ at $t=0$, at which the central density $\rho_c$ is $1.2\times10^{-4}$ in our unit. The dotted line and the dashed line indicate $M(J)$ at $t=42$ and 50, respectively, at which $\rho_c=1.2\times10^{-3}$ and $1.2\times10^{-1}$.

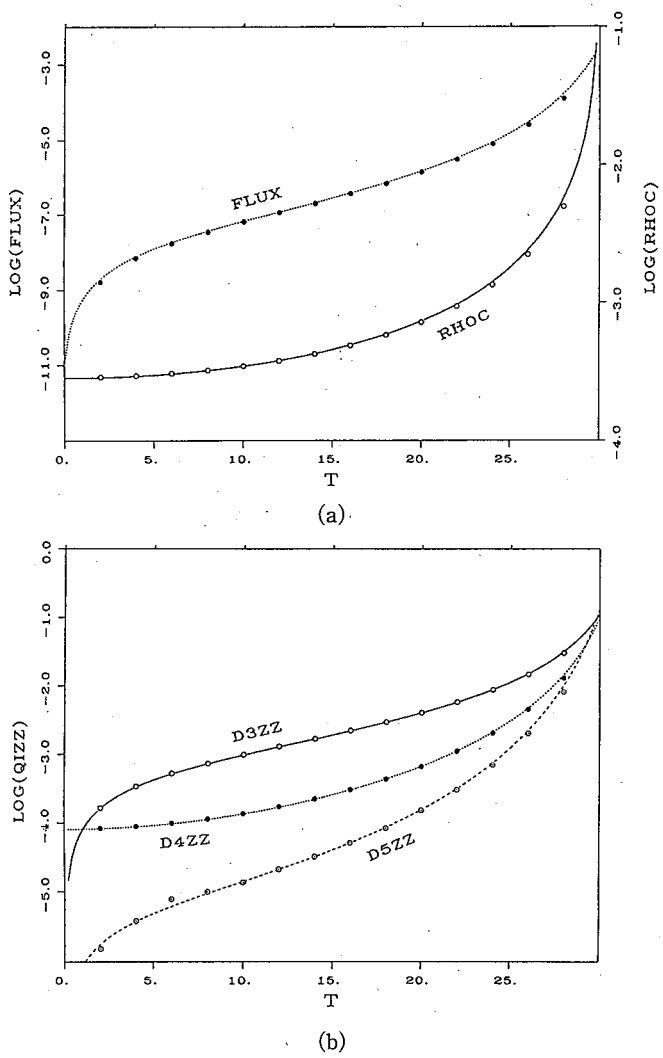


Fig. 9. Flux, central density and time derivatives of the quadrupole moment as functions of time for collapse of a triaxial homogeneous ellipsoid with initial semi-axes $a_1=12$, $a_2=10$ and $a_3=7$. The solid and the dotted line in (a) are semi-analytic results for the flux of the gravitational waves and the central density, respectively. The solid, the dotted and the dashed line in (b) are for the third, the fourth and the fifth derivatives of the quadrupole moment $\dddot{D}_{zz}$. The circles show the results obtained from the numerical simulation.

## Acknowledgements

The numerical calculations were performed on HITAC S820/80 at the Data Handling Center of National Laboratory for High Energy Physics (KEK). This work was in part supported by the Grant-in-Aid for Co-operating Scientific Research of Ministry of Education, Science and Culture (01306006, 01652509).

## Appendix A

*—— Method of Solving the Hydrodynamic Equation ——*

To integrate the hydrodynamics equation, we discretize Eqs. (2·1)~(2·3) as follows. Defining 4-dimensional vectors $Q$ and $F$ as

$$Q=\begin{pmatrix}\rho\\ \rho v^i\\ \rho\varepsilon\end{pmatrix}, \qquad F=\begin{pmatrix}0\\ \dfrac{\partial \tilde{P}_{ij}}{\partial x^j}+\rho\dfrac{\partial \psi}{\partial x^i}\\ \tilde{P}_{ij}\dfrac{\partial v^i}{\partial x^j}\end{pmatrix}, \tag{A·1}$$

then Eqs. (2·1)~(2·3) can be written as

$$\frac{\partial Q}{\partial t}+\frac{\partial Q v^j}{\partial x^j}=-F, \tag{A·2}$$

where $\tilde{P}_{ij}$ is the pressure tensor including the artificial viscosity given by Eq. (2·13). For transfer in the $x$-direction, the gradient of $Q$ and the velocity on each cell face at $n$-th time step are given by

$$\left(\frac{\partial Q}{\partial x}\right)^n_{i-1/2,j,k}=\frac{Q^n_{i,j,k}-Q^n_{i-1,j,k}}{x_i-x_{i-1}}\equiv\frac{Q^n_{i,j,k}-Q^n_{i-1,j,k}}{\Delta x_{i-1/2}}, \tag{A·3}$$

$$v^{x,n}_{i-1/2,j,k}=\frac{\rho^n_{i-1,j,k}v^{x,n}_{i-1,j,k}+\rho^n_{i,j,k}v^{x,n}_{i,j,k}}{\rho^n_{i-1,j,k}+\rho^n_{i,j,k}}. \tag{A·4}$$

We calculate the quantities transferred in the $x$-direction $\Delta Q^n_{i-1/2,j,k}$ by

$$\Delta Q^n_{i-1/2,j,k}=\{Q^n_{i-1,j,k}+(\nabla Q)^n_{i-1,j,k}(\Delta x_{i-1/2}-|v^{x,n}_{i-1/2,j,k}|\Delta t)\}\frac{v^{x,n}_{i-1/2,j,k}\Delta t}{\Delta x_{i-1/2}}, \tag{A·5}$$

if $v^{x,n}_{i-1/2,j,k}>0$ or

$$\Delta Q^n_{i-1/2,j,k}=\{Q^n_{i,j,k}-(\nabla Q)^n_{i,j,k}(\Delta x_{i-1/2}-|v^{x,n}_{i-1/2,j,k}|\Delta t)\}\frac{v^{x,n}_{i-1/2,j,k}\Delta t}{\Delta x_{i-1/2}}, \tag{A·6}$$

if $v^{x,n}_{i-1/2,j,k}<0$, where

$$(\nabla Q)^n_{i,j,k}=\begin{cases}0 & \text{if } \left(\dfrac{\partial Q}{\partial x}\right)^n_{i-1/2,j,k}\left(\dfrac{\partial Q}{\partial x}\right)^n_{i+1/2,j,k}\leq 0,\\ \min\left\{\left(\dfrac{\partial Q}{\partial x}\right)^n_{i-1/2,j,k}, \left(\dfrac{\partial Q}{\partial x}\right)^n_{i,j,k}, \left(\dfrac{\partial Q}{\partial x}\right)^n_{i+1/2,j,k}\right\} & \text{otherwise}\end{cases} \tag{A·7}$$

with

$$\left(\frac{\partial Q}{\partial x}\right)^n_{i,j,k}=\frac{1}{4}\left\{\left(\frac{\partial Q}{\partial x}\right)^n_{i-1/2,j,k}+\left(\frac{\partial Q}{\partial x}\right)^n_{i+1/2,j,k}\right\}. \tag{A·8}$$

For transfer in the $y$-direction and the $z$-direction, $\Delta Q^n_{i,j-1/2,k}$ and $\Delta Q^n_{i,j,k-1/2}$ are given in like manner. Then the density, momentum and energy density are advanced by

$$Q^{n+1}_{i,j,k}=Q^{n}_{i,j,k}-(\Delta Q^{n}_{i+1/2,j,k}-\Delta Q^{n}_{i+1/2,j,k})-(\Delta Q^{n}_{i,j+1/2,k}-\Delta Q^{n}_{i,j-1/2,k})$$
$$-(\Delta Q^{n}_{i,j,k+1/2}-\Delta Q^{n}_{i,j,k-1/2})-F^{n}_{i,j,k}\Delta t\ . \qquad (A\cdot 9)$$

In calculating $F^{n}_{i,j,k}$, the derivative of, for example, $\psi$ at a mesh point $(i, j, k)$ is given by

$$\left(\frac{\partial\psi}{\partial x}\right)_{i,j,k}=\frac{\psi_{i+1,j,k}-\psi_{i-1,j,k}}{x_{i+1}-x_{i-1}}\ . \qquad (A\cdot 10)$$

Equation (2·5) is integrated using ICCG method.[17]

## Appendix B
### —— *Code Testing* ——

We have performed various tests for our hydrodynamics code. We will show some of them here and will describe all tests in detail elsewhere.

The tests we performed include; (1) free transportation of a dust cube of a homogeneous or Gaussian density distribution. This test proved that the cube is successfully transported and no backscatter from the outer boundary appears. (2) Riemann shock tube. We have confirmed the one-dimensional shock tube is expressed by using the scheme described in Appendix A with the artificial viscosity terms given by Eq. (2·13). (3) Point explosion in the air. This test showed that a three-dimensional shock is successfully represented in our code and also that a spherically symmetric system is expressed satisfactorily using a Cartesian coordinate system.[13] (4) Local conservation of specific angular momentum for an axially symmetric collapse. (5) Collapse of a homogeneous ellipsoid. This test included comparison of third, fourth and fifth time derivatives of the quadrupole moment. In this appendix we show the results of (4) and (5).

We calculated collapse of a rotating dust sphere and checked the conservation of the specific angular momentum. Figure 8 shows the mass $M(J)$ with specific angular momentum less than or equal to $J$:

$$M(J)=\int_{j(x)\leq J}\rho(x)dV\ , \qquad (B\cdot 1)$$

where $j(x)$ is the specific angular momentum at a point $x$. The solid line in Fig. 8 indicates the initial value $M_0(J)$. The dotted line and the dashed line are respectively $M(J)$ at $t=42$ and 50 in our unit, at which the central density increases to about 10 and 1000 times of the initial density. All the lines fall on almost the same line in this figure, and the relative error

$$\Delta M(J)=\frac{M(J)-M_0(J)}{M_0(J)} \qquad (B\cdot 2)$$

is less than a few percent even at $t=50$.

As for checking the accuracy of time derivatives of the quadrupole moment, we calculated collapse of a triaxial homogeneous dust ellipsoid and compared the results with the semi-analytic ones, which are obtained through integration of ordinary differential equations.[14),15] Figures 9(a) and (b) show the comparison of the results

from the numerical simulation with the semi-analytic ones. The flux of the gravitational waves and the central density computed agree quite well with the semi-analytic solution until the central density increases by 100 times. This fact means that our code is satisfactory for the present problem. The third derivatives of the quadrupole moment are calculated by means of the method described in § 2 and the fourth and the fifth derivatives are calculated by means of the method mentioned in § 4. The computed values agree in general within 10% with the semi-analytic solutions. The accuracy for the fifth derivatives up to $t=7$ is not so good since the values of the fifth derivatives are very small compared with the values of the fourth derivatives. However such small components have little effects on the evolution of the system and the amount of the emitted gravitational waves.

**References**


1) D. G. Gilden and S. L. Shapiro, Astrophys. J. **287** (1984), 728.
2) L. Smarr, in *Sources of Gravitational Waves,* ed. L. Smarr (Cambridge University Press, Cambridge, 1979), p. 245.
3) R. F. Stark and T. Piran, Phys. Rev. Lett. **55** (1985), 891.
4) T. Nakamura, K. Oohara and Y. Kojima, Prog. Theor. Phys. Suppl. No. 90 (1987), 1.
5) J. P. A. Clark and D. M. Eardley, Astrophys. J. **215** (1977), 311.
6) J. H. Taylor, in *General Relativity and Gravitation 11,* ed. M. A. H. MacCallum (Cambridge University Press, Cambridge, 1987), p. 209.
7) J. G. Ables, in *Proceedings of the Fifth Marcel Grossmann Meeting on General Relativity,* ed. D. G. Blair and M. J. Buckingham (World Scientific, Singapore, 1989), (in press).
8) T. Nakamura and M. Fukugita, Astrophys. J. **337** (1989), 466.
9) P. Goldreich and D. Lynden-Bell, Mon. Not. R. A. Soc. **130** (1965), 97.
10) J. Kristian et al., Nature **338** (1989), 234.
11) T. Nakamura, Prog. Theor. Phys., **81** (1989), 1006.
12) L. S. Finn, in *Frontiers of Numerical Relativity,* ed. C. R. Evans, L. S. Finn and D. W. Hobill (Cambridge University Press, 1989), p. 126.
13) T. Nakamura and K. Oohara, ibid. p. 254.
14) S. Chandrasekhar, *Ellipsoidal Figures of Equilibrium* (Yale University Press, 1969).
15) S. L. Shapiro, in *Sources of Gravitational Radiation,* ed. L. L. Smarr (Cambridge University Press, 1979), p. 335.
16) J. LeBlanc, private communication.
17) K. Oohara and T. Nakamura, in *Frontiers of Numerical Relativity,* ed. C. R. Evans and L. S. Finn and D. W. Hobill,(Cambridge University Press, 1989), p. 74.
18) W. Misner, K. S. Thorne and J. A. Wheeler, *Gravitation* (W. H. Freeman and Company, San Francisco, 1970), p. 993.